Materials and Design 186 (2020) 108281

Contents lists available at ScienceDirect

Materials and Design

journal homepage: www.elsevier.com/locate/matdes

The effect of Bi on the microstructure, electrical, wettability and mechanical properties of Sn-0.7Cu-0.05Ni alloys for high strength soldering

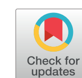

M.I.I. Ramli [a], M.A.A. Mohd Salleh [a,*], H. Yasuda [b], J. Chaiprapa [c], K. Nogita [d]

[a] Center of Excellence Geopolymer & Green Technology (CeGeoGTech), School of Materials Engineering, Universiti Malaysia Perlis (UniMAP), Taman Muhibbah, 02600, Jejawi, Arau, Perlis, Malaysia
[b] Department of Materials Science and Engineering, Kyoto University, Sakyo-ku, Kyoto, 606-8501, Japan
[c] Synchrotron Light Research Institute, Muang, Nakhon Rathasima, 3000, Thailand
[d] Nihon Superior Centre for the Manufacture of Electronic Materials (NS CMEM), School of Mechanical and Mining Engineering, The University of Queensland, Brisbane, QLD, 4072, Australia

HIGHLIGHTS

- The microstructure, electrical, wettability and mechanical properties of the Sn-0.7Cu-0.05Ni-Bi were revealed.
- The Micro-XRF analysis had shown the well-distributed Bi element in the β-Sn of the Sn-0.7Cu-0.05Ni-Bi solder joint.
- $(Cu,Ni)_6Sn_5$ primary intermetallic in the Sn-0.7Cu-0.05Ni-1.5Bi/Cu was discovered to result in a rapid early growth rate.
- The addition of 1.5%Bi was found to have resulted in an improved of electrical conductivity and wettability performance.
- The shear strength of the solder joints was revealed to increase with the addition of 1.5 wt.% Bi.

GRAPHICAL ABSTRACT

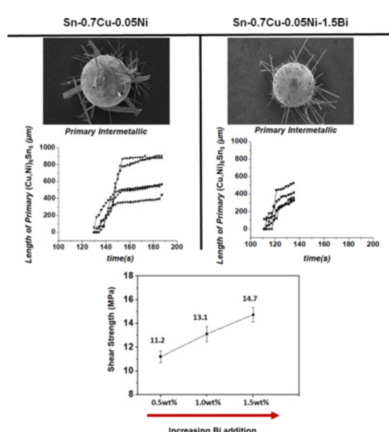

ARTICLE INFO

Article history:
Received 18 June 2019
Received in revised form 12 September 2019
Accepted 15 October 2019
Available online 18 October 2019

Keywords:
Soldering
Solder
Interconnects
Intermetallics
Solid solution

ABSTRACT

This paper elucidated the effects of the Bi element (0 wt%, 0.5 wt% and 1.5 wt%) on the microstructure, electrical, wettability and mechanical properties of the Sn-0.7Cu-0.05Ni as a high strength solder. Besides using the conventional cross-sectioned microstructure image, the real-time synchrotron radiation imaging and synchrotron micro-X-ray fluorescence (XRF) technique was also used to investigate the microstructure, focusing on the *in-situ* growth behaviour of the primary $(Cu,Ni)_6Sn_5$ intermetallic and elemental distribution that had occurred in the Sn-0.7Cu-0.05Ni-1.5Bi. Other essential properties of solder material, such as wettability, electrical resistance, and shear strength, were also determined. The results showed that the addition of 1.5 wt% Bi refined the primary $(Cu,Ni)_6Sn_5$ intermetallics formation in the solder joint, where it grew earlier and faster relative to that in the Sn-0.7Cu-0.05Ni/Cu joint. Additionally, the addition of 1.5 wt% Bi resulted with a 3% reduction of its electrical resistance while increasing the wettability of the solder alloy. 1.5 wt% addition of the Bi element also found to have contributed to a significant increment of shear strength relative to that of the Sn-0.7Cu-0.05Ni. The results

* Corresponding author.
E-mail addresses: mohdizrulizwan@gmail.com (M.I.I. Ramli), arifanuar@unimap.edu.my (M.A.A. Mohd Salleh), yasuda.hideyuki.6s@kyoto-u.ac.jp (H. Yasuda), jitrin@slri.or.th (J. Chaiprapa), k.nogita@uq.edu.au (K. Nogita).

https://doi.org/10.1016/j.matdes.2019.108281
0264-1275/© 2019 The Authors. Published by Elsevier Ltd. This is an open access article under the CC BY-NC-ND license (http://creativecommons.org/licenses/by-nc-nd/4.0/).

Microstructure
Solder properties

confirmed that the developed material is applicable as a potential high strength solder material in the context of advanced interconnecting applications.

© 2019 The Authors. Published by Elsevier Ltd. This is an open access article under the CC BY-NC-ND license (http://creativecommons.org/licenses/by-nc-nd/4.0/).

1. Introduction

The eutectic Sn-0.7Cu solder alloy is commonly for electronics interconnect applications in wave and reflow soldering due to its availability and cost-effectiveness. However, its mechanical and wettability properties are known to be dismal, owing to the growth of a brittle intermetallic compound (IMC) and the large primary Cu_6Sn_5 crystals in its solder matrix. These factors prompted many studies to focus on the addition of microalloying elements such as Ni [1–6], Zn [7,8], Bi [9–12], P [13] and Al [14,15] in the Sn-0.7Cu solder system. It was subsequently confirmed that the addition of small amounts of Ni (to the Sn-0.7Cu solder alloy) significantly affected its solidification behaviour and intermetallic morphologies [1,16], but also decreased bridging and improved drainage and wettability [17]. This was confirmed by Ventura et al. [18] and Nogita et al. [19], whom reported that the addition of a 500 ppm of the Ni element in the Sn-0.7Cu solder alloy as stabilizing the hexagonal $(Cu,Ni)_6Sn_5$ phase and preventing the volumetric changes from contributing to the cracking of the Ni-free alloys, hence producing a better Sn-0.7Cu-0.05Ni-based solder with enhanced solder properties.

One of the methods for improving the mechanical properties of an alloying element is via solid solution strengthening, where atomic addition to a crystalline lattice results in high distortion, which increases the yield stress of the subsequent material [20]. Alloying elements such as Bi, Ga and Sb are known to affect solid solution strengthening in Sn alloys, The Bi element, for example, is commonly used for lowering the liquidus temperature, which improves the mechanical properties of the subsequent solder joints in harsh setting [21–25]. Since most electronic components in the automotive and defence industries are exposed to harsh environments, it would seem prudent to account for this in the designs of the high-strength solid solution solder joint to address such environments. Mahdavifard et al. [9] reported that the additions of the Bi element to the Sn-1.0Ag-0.5Cu-Fe solder increases its yield and ultimate strength while decreases the Cu_6Sn_5 and increases the β-Sn content in the solder, while Hu et al. [26] reported that the addition of a similar alloying element as enhancing the mechanical properties and solderability of the Sn-0.7Cu solder. Adding higher amount of Bi for solid solution strengthening may lead to a more brittle solder, contrasting with the typical requirements of high strength solder joint materials. As reported by Liu et al. [27], the high amount of Bi addition may lead to a brittle solder material. This Sn-0.7Cu-0.05Ni-xBi solder alloy is lower cost compared to Sn-3.0Ag-0.5Cu solder alloy (most widely used in current market) in term of material, where the composition does not contain expensive elements such as Ag. Since the microstructure analysis of a developing solder forms a pivotal point of this study, a more advanced technique is therefore required for analysing the microstructural growth of the various developed solder alloys. The synchrotron radiation imaging technology has emerged as a powerful tool for observing detailed *in situ* solidification of alloys [28,29], hinging on the fact that previous studies had successfully utilised the technique in their intermetallic phase growth and morphology research during soldering [10,28,30–33]. The large intermetallic compounds such as Cu_6Sn_5 and Ag_3Sn are undesirable for solder alloys because their formation can be related to crack initiation [34,35]. Thus smaller primary $(Cu,Ni)_6Sn_5$ crystal may improve the mechanical reliability of a solder joint. In previous study, Mohd Salleh et al. [35] had discovered the addition of the Ni element as affecting the primary $(Cu,Ni)_6Sn_5$ growth on the Sn-0.7Cu/Cu joints during the soldering process. In another study, by using the synchrotron imaging technique, they also discovered the formation of the Cu_6Sn_5 growth in the Sn-3.0Ag-0.5Cu solder alloys [30]. The influence of the Bi element on the Sn-0.7Cu-0.05Ni has not been elucidated via *in situ* synchrotron imaging technique. Additionally, other solder properties such as wettability and electrical resistance of the Bi-added Sn-0.7Cu-0.05Ni solder system has not been widely reported.

Current research has renewed interest in the microstructure formations of the first IMC growth kinetics of primary $(Cu,Ni)_6Sn_5$ since the morphologies and distributions of the IMC formed during the soldering process were found to have subsequently dictated the mechanical

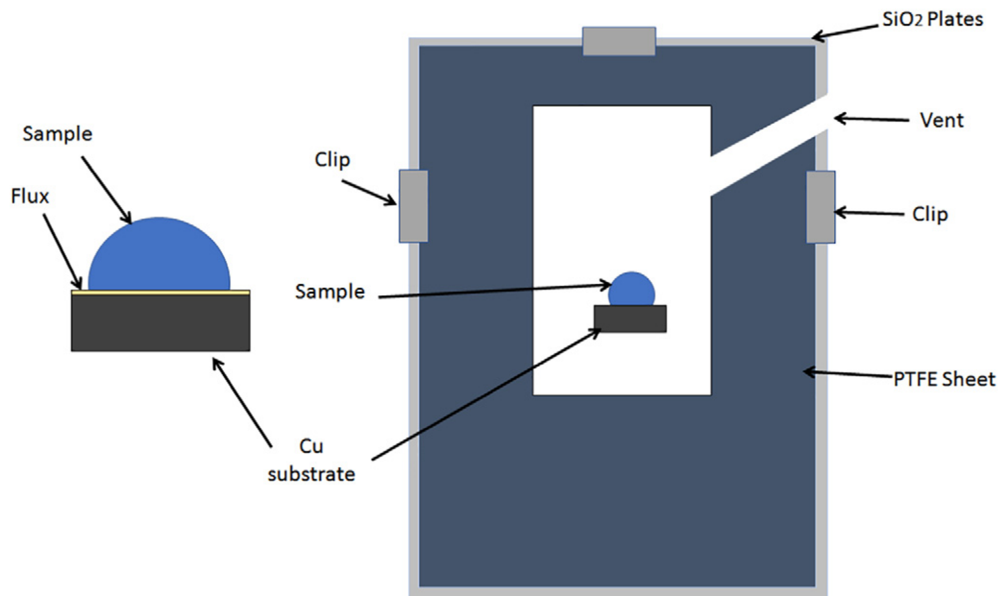

Fig. 1. The setup of a soldering sample cell for the real-time synchrotron solidification process (Figure is not drawn to scale).

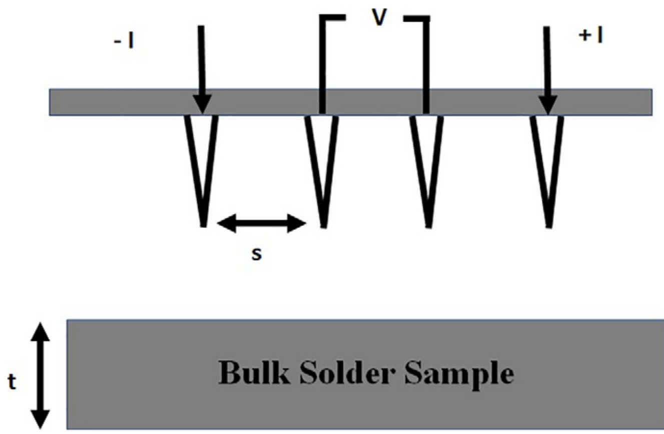

Fig. 2. Schematic diagram of the 4-point probe configuration.

properties of the solder joints [36]. Since the IMC plays an essential role in the predicting the reliability of the solder joints [30], an investigation is therefore required to elucidate the effect of the added Bi element on the Sn-0.7Cu-0.05Ni solder joint. By using the synchrotron real-time imaging technique, this approach will not only be helpful for analysing the influence of the Bi element on the formation and growth kinetics of the primary $(Cu,Ni)_6Sn_5$ IMCs in the Sn-0.7Cu-0.05Ni solder alloy during the solidification process, but can also be utilised to observe the nucleation, growth rate and growth direction of the primary (Cu,Ni)6Sn5 crystals during soldering. Apart from conducting the above in-situ observation as well as the effect of the Bi element on the wettability, electrical resistance, shear strength and the fracture surface of the solder alloys, the distribution of the Bi element in the Sn-0.7Cu-0.05Ni solder alloy can also be determined using the synchrotron micro-XRF as an approach of gauging its solid solution strengthening effect on the solder's microstructure and joint strength.

2. Experimental procedure

2.1. Sample preparation

The alloy was prepared by melting the Sn-0.7Cu-0.05Ni ingots that had been supplied by Nihon Superior Co. Ltd. in a graphite crucible. Three different solder compositions, based on their respective Bi contents (0 wt%, 0.5 wt% and 1.5 wt%), namely the Sn-0.7Cu-0.05Ni, Sn-0.7Cu-0.05Ni-0.5Bi and Sn-0.7Cu-0.05Ni-1.5B, were prepared by suspending them for 1 h in an electric-resistance furnace at a temperature of 350 °C. Once this process had been completed, the molten solder was then stirred with a pre-heated graphite rod and poured into stainless steel moulds that would be eventually cooled to the room temperature. The solder balls with a diameter of 600 μm, which had been produced with a 2.0 mm diameter metal punch from the alloy foils that had been rolled to a 30 μm thickness, were then dipped with a rosin mildly activated (RMA) flux and melted in a reflow oven at 250 °C for 60 s. Surface tension forced the formation of these solder balls, which were further passed through a series of sieves to ensure size uniformity.

2.2. Microstructure analysis

The solder balls with a small amount of RMA flux were then placed on a Cu substrate printed board (PCB) with an organic soldering preservative (OSP) surface finish and were heated to ~250–°C at 0.33–°C/s for

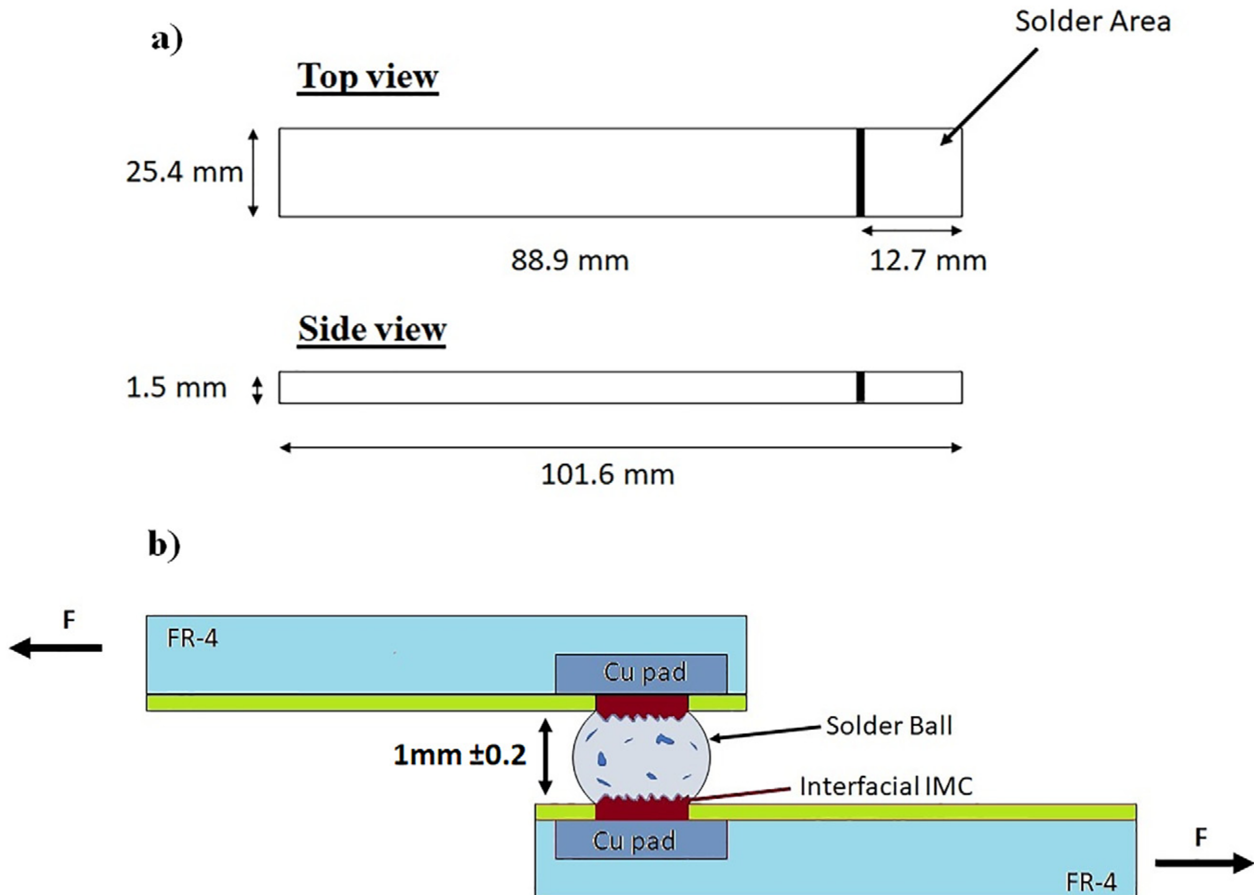

Fig. 3. (a) Specifications of the shear test specimen and (b) Schematic drawing of the solder joints shear test.

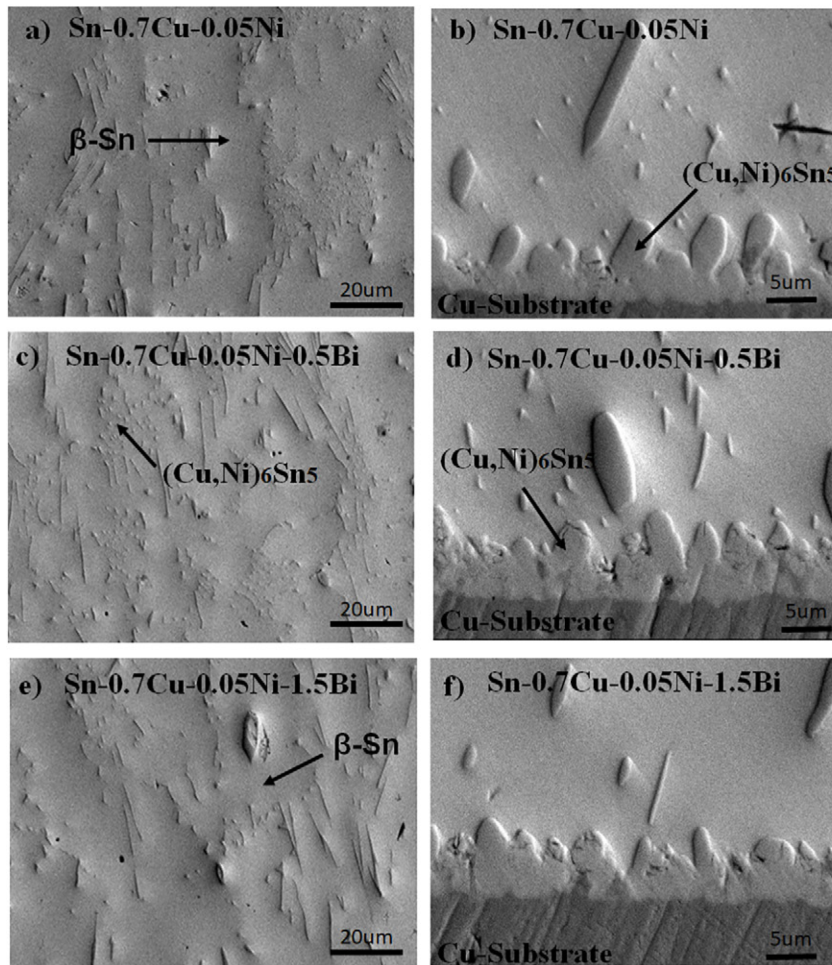

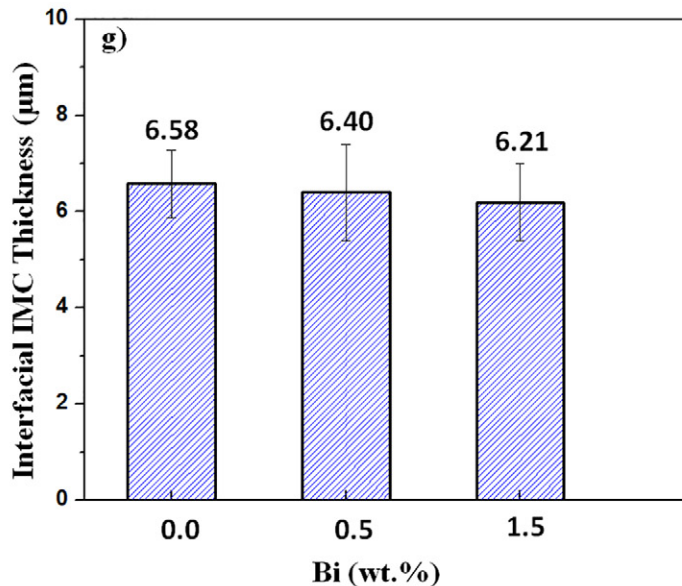

Fig. 4. The microstructures of the primary and interfacial IMCs of (a and b) Sn-0.7Cu-0.05Ni, (c and d) Sn-0.7Cu-0.05Ni-0.5Bi, and (e and f) Sn-0.7Cu-0.05Ni-1.5Bi solder alloy, and (g) influence of Bi addition to the interfacial IMC thickness.

30–s before being cooled down at ~0.33–°C/s. To conduct the conventional cross-sectioned images, the reflowed samples were first mounted in epoxy resin and grounded with the SiC paper before they were mechanically polished to 0.05–μm by using the colloidal silica suspension. The microstructural analysis of the three-dimensional primary IMC that was produced by etching the solder joints with a 93% methanol +5%HNO_3 + 2%HCl solution was then conducted using a scanning electron microscope (SEM). Further analysis on the primary IMC growth kinetics of primary $(Cu,Ni)_6Sn_5$ and the elemental distribution mappings was then performed using the synchrotron X-ray radiography imaging and the synchrotron micro-X-ray fluorescence (XRF), respectively.

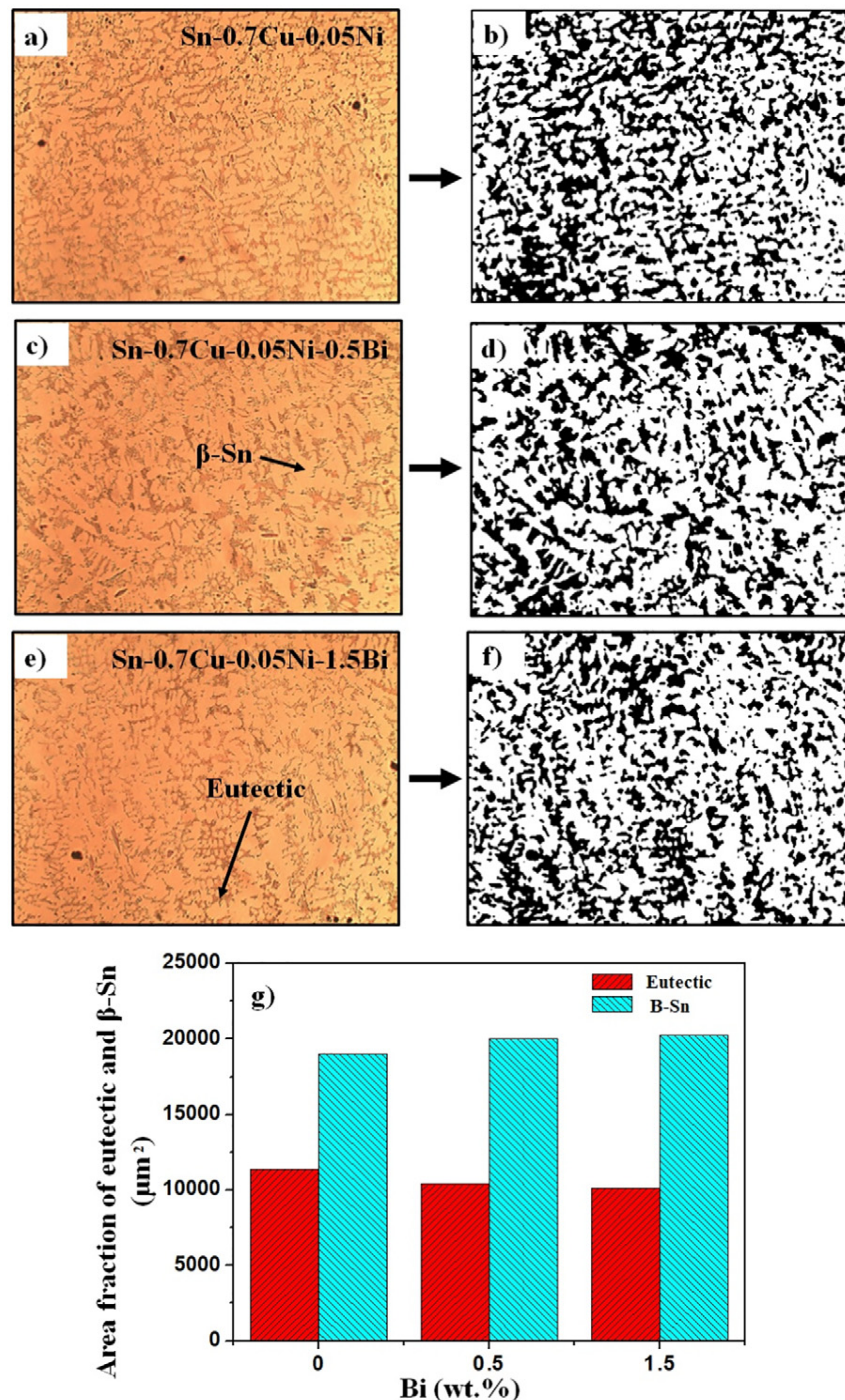

Fig. 5. The microstructure of bulk solder before and after threshold process at (a and b) Sn-0.7Cu-0.05Ni, (c and d) Sn-0.7Cu-0.05Ni-0.5Bi, and (e and f) Sn-0.7Cu-0.05Ni-1.5Bi solder alloy and (g) area fraction of the eutectic $(Cu,Ni)_6Sn_5$ and β-Sn dendrites.

2.2. Synchrotron X-ray radiography imaging

The real-time synchrotron radiation imaging experiments were performed at SPring-8, which is a large synchrotron radiation facility located in Japan. Detailed experimental setup of the schematic diagram shown in Fig. 1 were derived from Refs. [30,35,37]. The 600 μm diameter Sn-0.7Cu-0.05Ni and Sn-0.7Cu-0.05Ni-1.5Bi solder balls, Cu substrates and the rosin-based flux were first layered vertically and sandwiched between the SiO_2 glass plates and PTFE sheets prior being heated in a furnace to an ~250 °C at 0.33 °C/s for 30 s and cooled at ~0.33 °C/s. A camera with a resolution ratio of 2.74 μm per pixel and an exposure time of 0.5 s/frame was then used to capture and collect images from the sample's solidification process, while an X-ray energy of 21 KeV between the edges was selected to create a higher contrast between the primary and secondary phases [35].

2.3. Synchrotron micro-X-ray fluorescence (XRF)

The synchrotron μ-XRF experiments that were performed at the Synchrotron Light Research Institute (SLRI) in Thailand used the BL6b

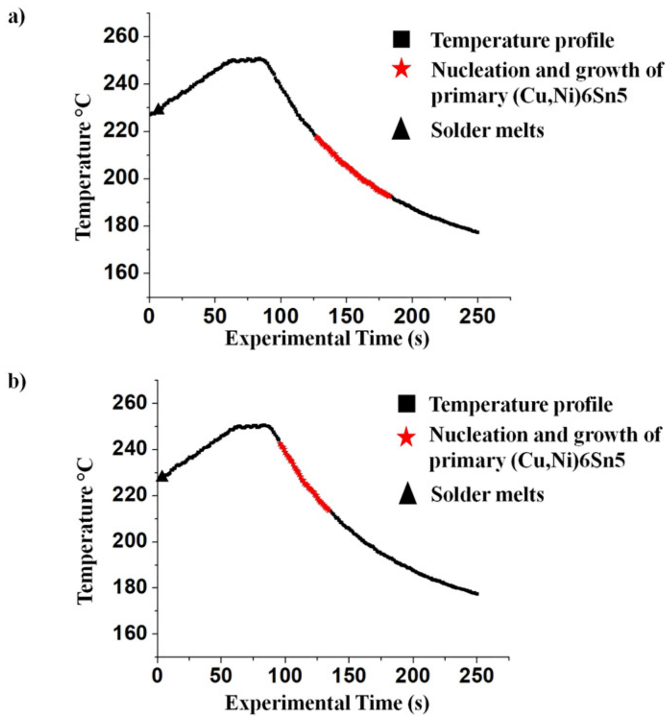

Fig. 6. Temperature profile and growth behaviour of the primary $(Cu,Ni)_6Sn_5$ (a) Sn-0.7Cu-0.05Ni, and (b) Sn-0.7Cu-0.05Ni-1.5Bi. Experimental time = 0 when the solder had started to melt.

beamline, where the size of the white X-ray beam that was produced from a bend magnet was limited by a circular aperture and focused using a polycapillary lens to generate a 30×30 μm^2 X-ray beam size on the specimen. Without a monochromator, the energy of the micro X-ray beam would have been 2–12 keV. The specimen was then placed at a 90° level between the X-ray beam and the ccd camera, while the Vortex EM-650 silicon drift detector that was used to amass the emitted fluorescent X-rays from the samples was positioned with a 45° to the specimen. These specimens were mounted vertically on the sample holder and scanned at a rapid rate using the high precision motorized stages. The results were then analysed with the PyMca software [38] once the experiments were completed for each of the point in the air atmosphere with a 30 s exposure time and a step size of 0.05 mm.

2.4. Wettability analysis

The solder's wettability was determined based on it's contact angle. After the solder ball had been placed on a Cu-substrate with a no-clean flux and heated ~250 °C at 0.33 °C/s 30 s before being cooled down at ~0.33 °C/s, the wetting contact angle θ, was then measured from the spreading sample that had been bisected, which would be then cross-sectioned, mounted, and ground with multiple grit size SiC paper.

2.5. Electrical resistance

The electrical resistance (ρ) of the Sn-0.7Cu-0.05Ni-xBi solder alloys were measured using the four-point Keithley probe. This approach has the advantage of enabling the measurement of sample resistance without the interference of a contact resistance. The size of the samples used in this measurement was of 1.2 cm in diameter and 3 cm length, with a probe spacing of 0.5 cm, while the corresponding voltage that had dropped across the sample was measured with a 2A current. A total of five samples were tested for each composition. Since the sample thickness (t) is greater than the probe spacing (s), the equation below was used to calculate the sample's electrical resistivities.

$$\rho = 2\pi s\left(\frac{V}{I}\right) \tag{1}$$

ρ is resistivity, π is 3.42, s is the probe spacing, v is voltage and I is current. A schematic diagram of the four-point probe configuration that was used for measuring the electrical resistance of the solder alloys is shown in Fig. 2.

2.6. Shear strength test

The strength of the solder that was bonded on the Cu-substrate (PCB FR-4 type) was subsequently analysed using the solder joint test. The 1 g

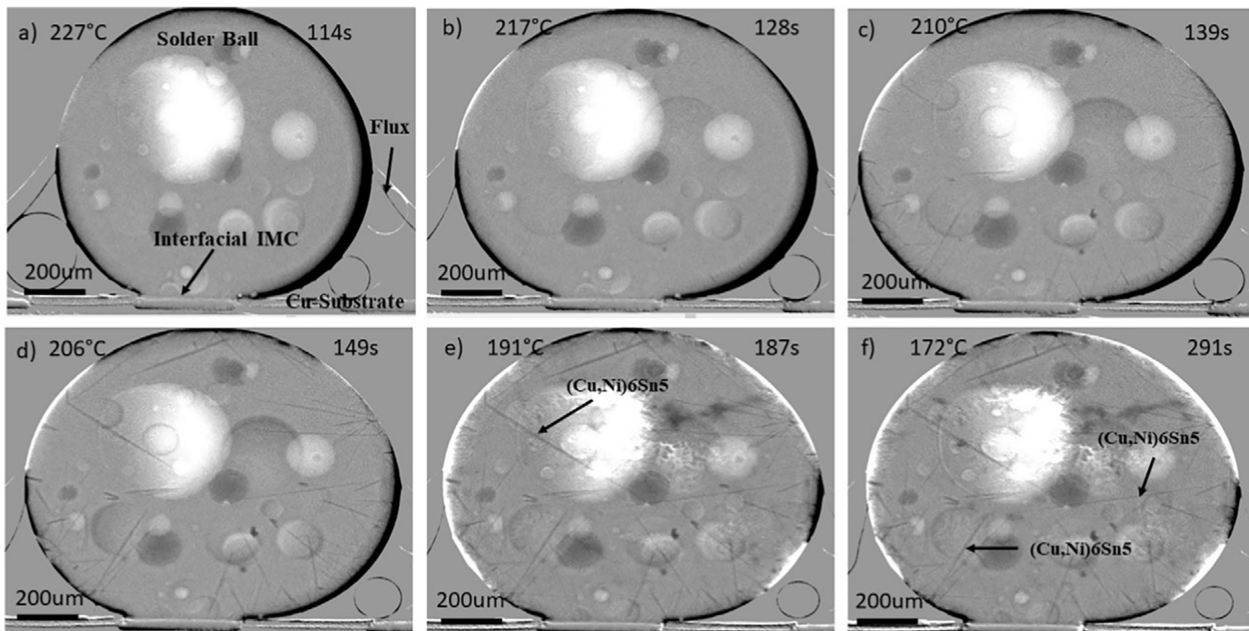

Fig. 7. Real-time observations of the microstructural development that had occurred during the Sn-0.7Cu-0.05Ni and Cu substrate solidification process with the experimental times of (a) 114 s, (b) 128 s, (c) 139 s, (d) 149 s, (e) 187 s and (f) 291 s t = 0 when the solder had started to melt.

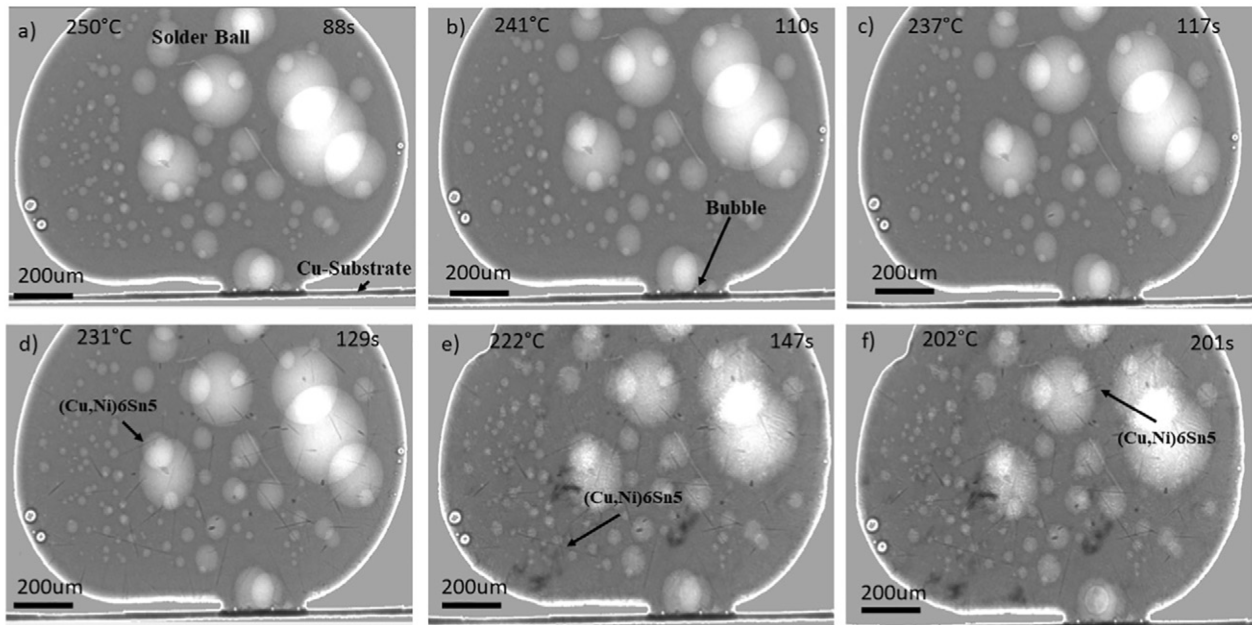

Fig. 8. Real-time observations of the microstructural development that had occurred during the Sn-0.7Cu-0.05Ni-1.5Bi and the Cu substrate solidification process with the experimental times of (a) 88 s, (b) 110 s, (c) 117 s, (d) 129 s, (e) 147 s and (f) 201 s t = 0 when the solder had started to melt.

of solder alloy and the rosin-based flux were layered vertically and sandwiched with the Cu-substrate and heated to ~250 °C at 0.33 °C/s for 30 s before being cooled at ~0.33 °C/s. An Instron machine was then used to conduct the shear test on the Cu-substrate, which was pre-set as per the ASTM D1002 specification shown in Fig. 3a. The fracture surface of the solder joint was analysed in the context of two shear loads at opposing directions of 2 mm/min, as illustrated in Fig. 3b. The thickness of the solder was ~1 mm ± 0.2, and the five samples for each composition was used to calculate the accuracy of the average values.

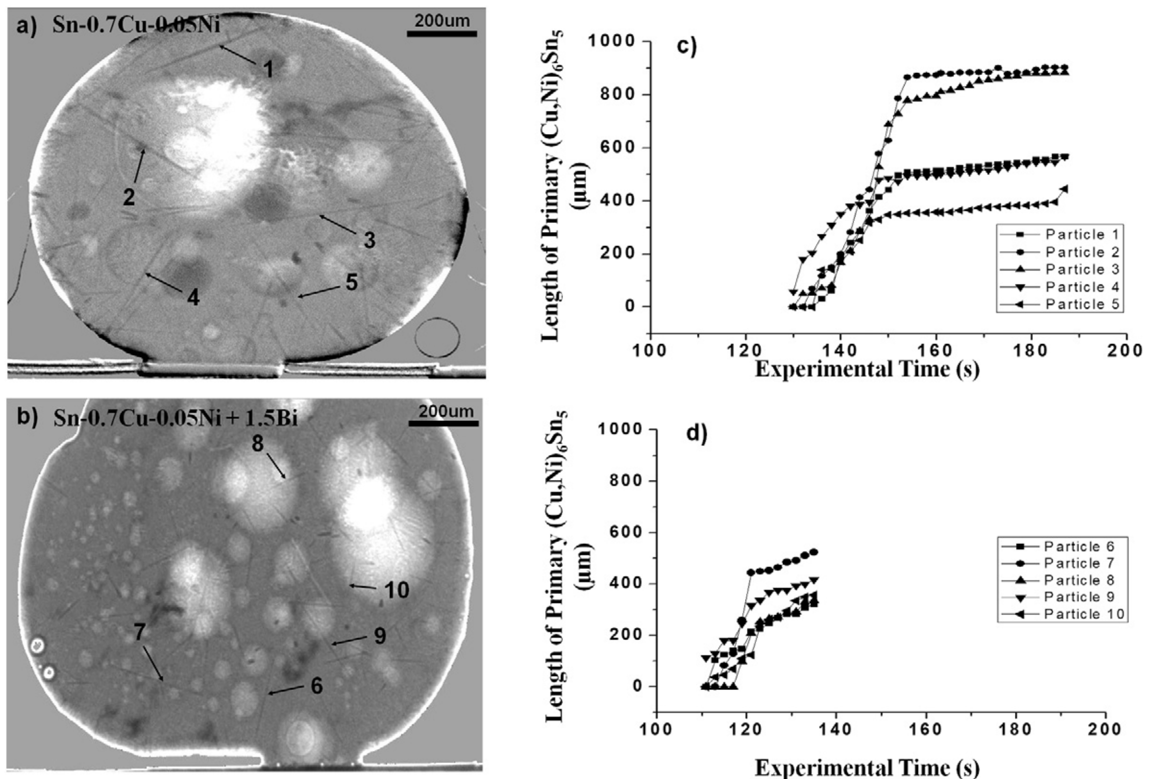

Fig. 9. (a and b) the typical individual primary intermetallics that were chosen for the measurement study. The growth evolution of the primary intermetallics that had existed in the (c) Sn-0.7Cu-0.05Ni and (d) Sn-0.7Cu-0.05Ni-1.5Bi solder joints during the cooling process.

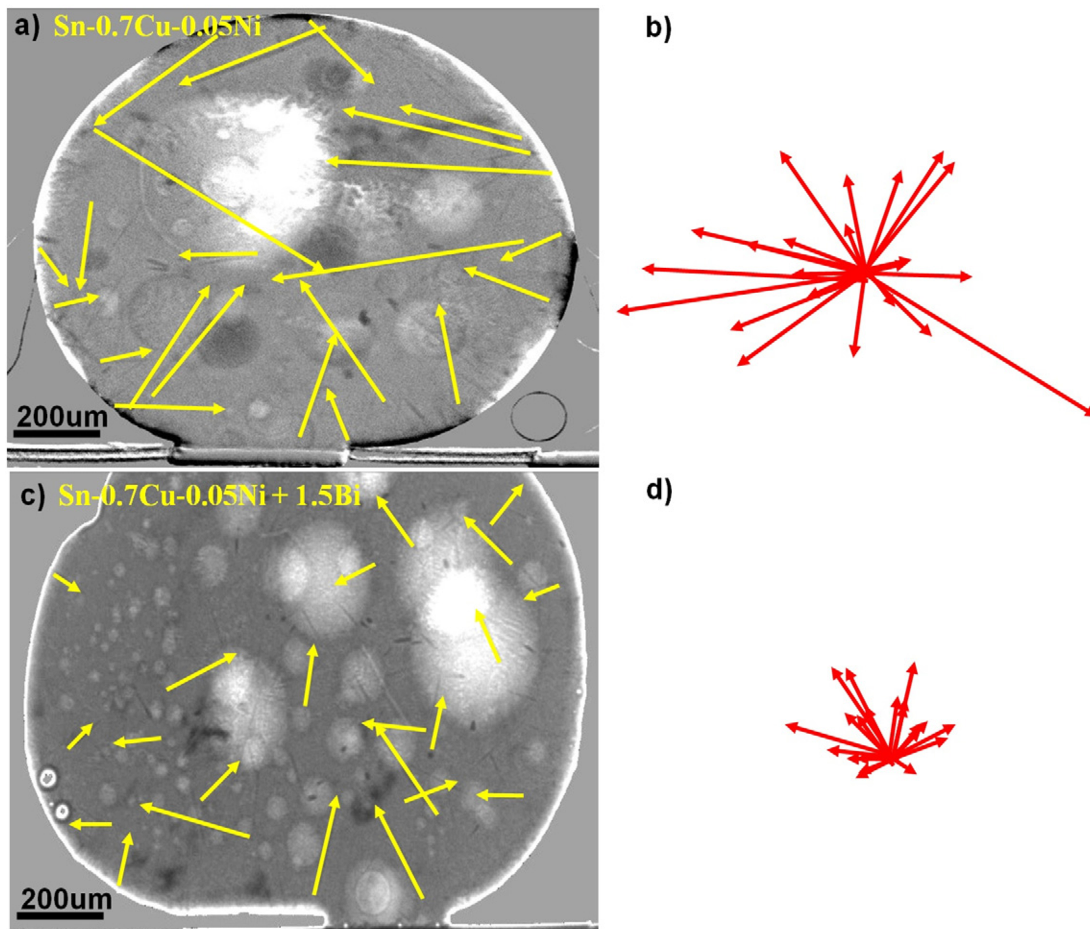

Fig. 10. (a and c) shows the growth vectors of the (Cu,Ni)6Sn5 that had appeared in the Sn0.7Cu0.05Ni/Cu and Sn0.7Cu0.05Ni1.5Bi/Cu solder joints and (b and d) the same vectors with an origin that shows the distributed growth orientation.

3. Results and discussion

3.1. Microstructures of the interfacial intermetallic (IMC) and eutectic intermetallic compounds

The microstructures of the solidified Sn-0.7Cu-0.05Ni/Cu and Sn-0.7Cu-0.05Ni-xBi/Cu solder joints are shown in Fig. 4. While the cross-sectioned image of the eutectic IMC, as depicted in Fig. 4a, c, e, confirmed the presence of β-Sn and $(Cu,Ni)_6Sn_5$ phases in the solder bulk region, those of the interfacial IMC were found to have formed on the Cu substrate, as per Fig. 4b, d, f. This therefore indicates that the eutectic IMC in the Sn-0.7Cu-0.05Ni were refined and its size slightly suppressed due to the addition and subsequent presence of the Bi element.

The interfacial reaction between the Sn from the solder and Cu substrate in the formation of the $(Cu,Ni)_6Sn_5$ was found to be necessary for the formation of the metallurgical bond after the reflow process. Despite the Sn-0.7Cu-0.05Ni interfacial thickness showing a slight decrease from 6.58 μm to 6.21 μm due to the addition of a 1.5 wt%Bi, the interfacial IMC layer of the Sn-0.7Cu-0.05Ni was however not found to have been affected by the 0.5 wt% and 1.5 wt% Bi elements, as shown in Fig. 4b,d,f. In this study, we don't see any Cu_3Sn formation at the interfacial IMC. Cu_3Sn typically forms in a Sn-Cu solder joint in an alloy such as Sn-0.7Cu and will increase in size/thickness if the solder joint is subsequently aged. During soldering and solidification of the Sn-Cu solder joint, Cu_6Sn_5 will form by the dissolution of Cu. According to the Cu-Sn phase diagram, the liquidus temperature of reactions leading directly to Cu_6Sn_5 formation is above 227 °C, while the liquidus temperature of those leading to Cu_3Sn is above 415 °C. Therefore, at 260 °C, Cu_6Sn_5 is a direct reaction product between Cu and liquid Sn, but Cu_3Sn could only be obtained from a solid-state reaction between Cu and Cu_6Sn_5 [39]. In addition, it indicates that the Cu_3Sn phase forms only when the crystallization temperature of the system reaches 415 °C or above. During isothermal aging, the Cu_6Sn_5 phase in the layer grows by interdiffusion of Cu and Sn and reaction with each other, while the Cu_3Sn phase forms and grow by reactions between the Cu substrate and Cu_6Sn_5 phase IMC layer [40]. The Cu_3Sn intermetallic is avoided because of its brittle nature that can decrease the shear strength of a solder joint. From previous study [41], it is known that Ni were able to suppress the formation of Cu_3Sn. In addition, it has been previously shown that small concentrations of Bi (~1%) in the Sn-Ag-Cu alloys can significantly retard the kinetics of Cu_3Sn formation at the Cu-solder interface [42]. As such, the small concentrations of Bi (0.5–1.5%) could be the reason for the non-observance of this intermetallic in the present case. Fig. 4g show the interfacial IMC layers of the Sn-0.7Cu-0.05Ni and Sn-0.7Cu-0.05Ni-1.5Bi being thinner than those of the Sn-0.7Cu [35] and Sn-3.0Ag-0.5Cu [30], respectively. However, Belyakov et al. [43] discovered the gradual decrease of the IMC layer thickness from the addition of 14 wt% Bi in the Sn-0.7Cu-0.05Ni resulted from the reduced Cu solubility, which had slowed the reaction rate between the molten solder and the Cu substrate [24]. Despite Bi element not significantly influencing the eutectic and interfacial IMC chemical composition [44], its presence in the bulk solder can, however, be regarded as providing a solid solution strengthening mechanism to the solder joint.

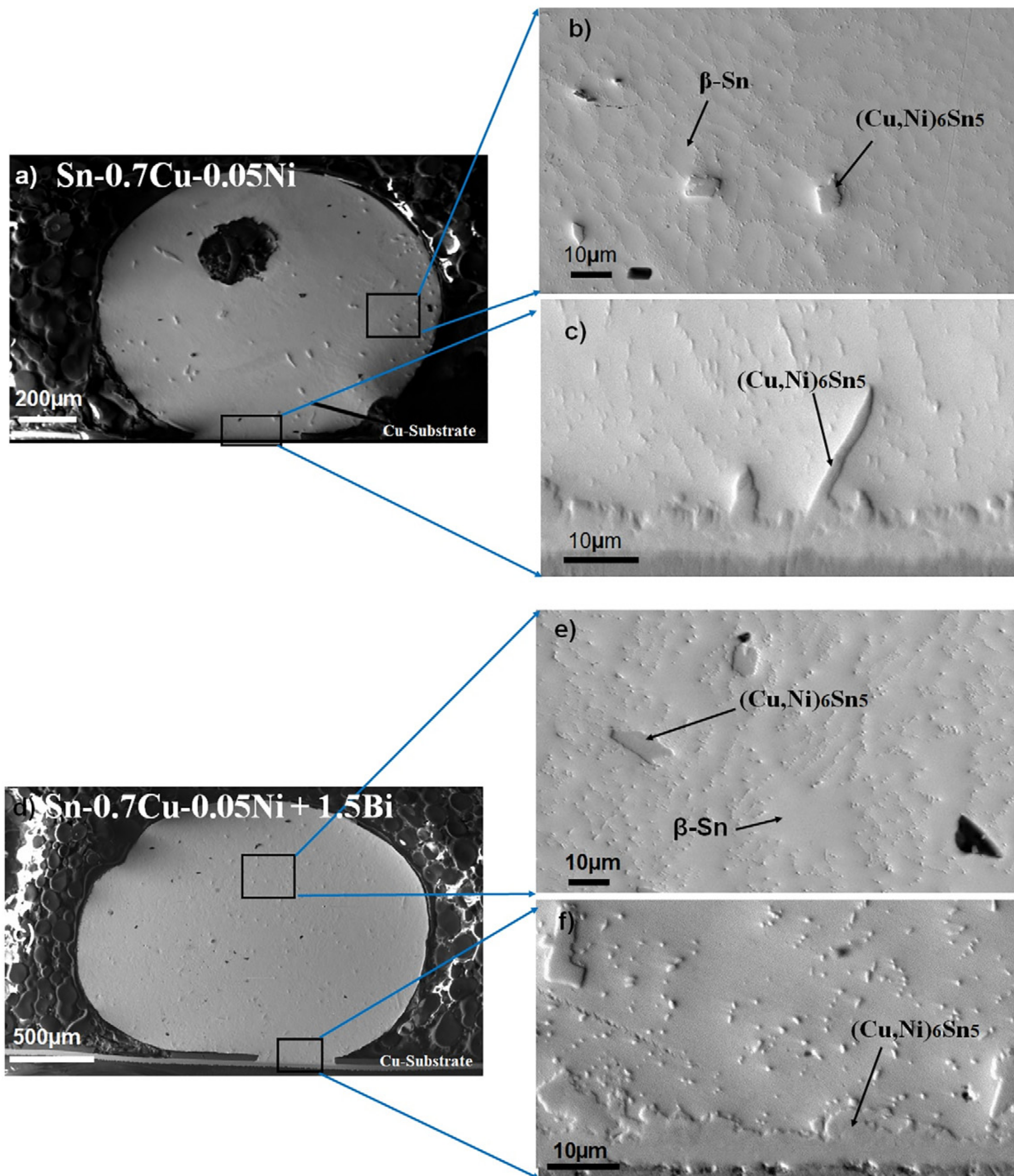

Fig. 11. Post mortem samples of the (a) Sn-0.7Cu-0.05Ni/Cu with (b) primary $(Cu,Ni)_6Sn_5$ IMC and (c) interfacial $(Cu,Ni)_6Sn_5$ IMC layers. Post mortem samples of the (d) Sn-0.7Cu-0.05Ni-1.5Bi/Cu with (e) primary $(Cu,Ni)_6Sn_5$ IMC and (f) interfacial $(Cu,Ni)_6Sn_5$ IMC layers.

3.2. Area fraction of the eutectic $(Cu,Ni)_6Sn_5$ and β-Sn

The area fraction of the eutectic $(Cu,Ni)_6Sn_5$ and β-Sn that had been quantitatively analysed by using the image-J software with its area fraction and the β-Sn dendrites, as well as its microstructural changes are shown in Fig. 5b,d,f and Fig. 5g, respectively. As per these figures, the addition and present of the Bi element were found to have minimally affected the β-Sn and eutectics area fraction as the additions were confirmed to have only slightly increased and decreased the respective β-Sn and the $(Cu,Ni)_6Sn_5$ area fraction of the Sn-0.7Cu-0.05Ni solder alloy. These slight changes may have been due to the addition of the Bi element within the β-Sn matrix, which had curtailed the chemical reaction of the Sn activity during the solidification process. As the precipitation of the Bi-rich particles had not been observed in the solder alloys, this would have implied that the Bi element had dissolved into the supersaturation of the primary β-Sn phase, while the Bi solder alloys microstructure that had composed of the β-Sn phase and Cu-Sn IMC would have been attributed to the high solubility of the Bi element in the Sn. The presence of the Bi element can also be assumed to have minimal effect on the eutectic $(Cu,Ni)_6Sn_5$ IMC area fraction and the β-Sn dendrites area fraction, as per Mahdavifard et al. [22], who posited that the addition of the Bi element in the Sn-1.0Ag-0.5Cu-Fe resulted in a slight increase and decrease of the β-Sn and the Cu_6Sn_5, respectively. However, Liu et al. [27] contradicted this by positing that the addition of the Bi element in the Sn-Ag-Cu solder to increase the area fraction and size of the β-Sn dendrites.

3.3. Growth behaviour of the primary $(Cu,Ni)_6Sn_5$

The growth behaviour of the $(Cu,Ni)_6Sn_5$ IMC on the Cu-substrate interface during the soldering process was elucidated using the real-time synchrotron radiation imaging technology. From the temperature

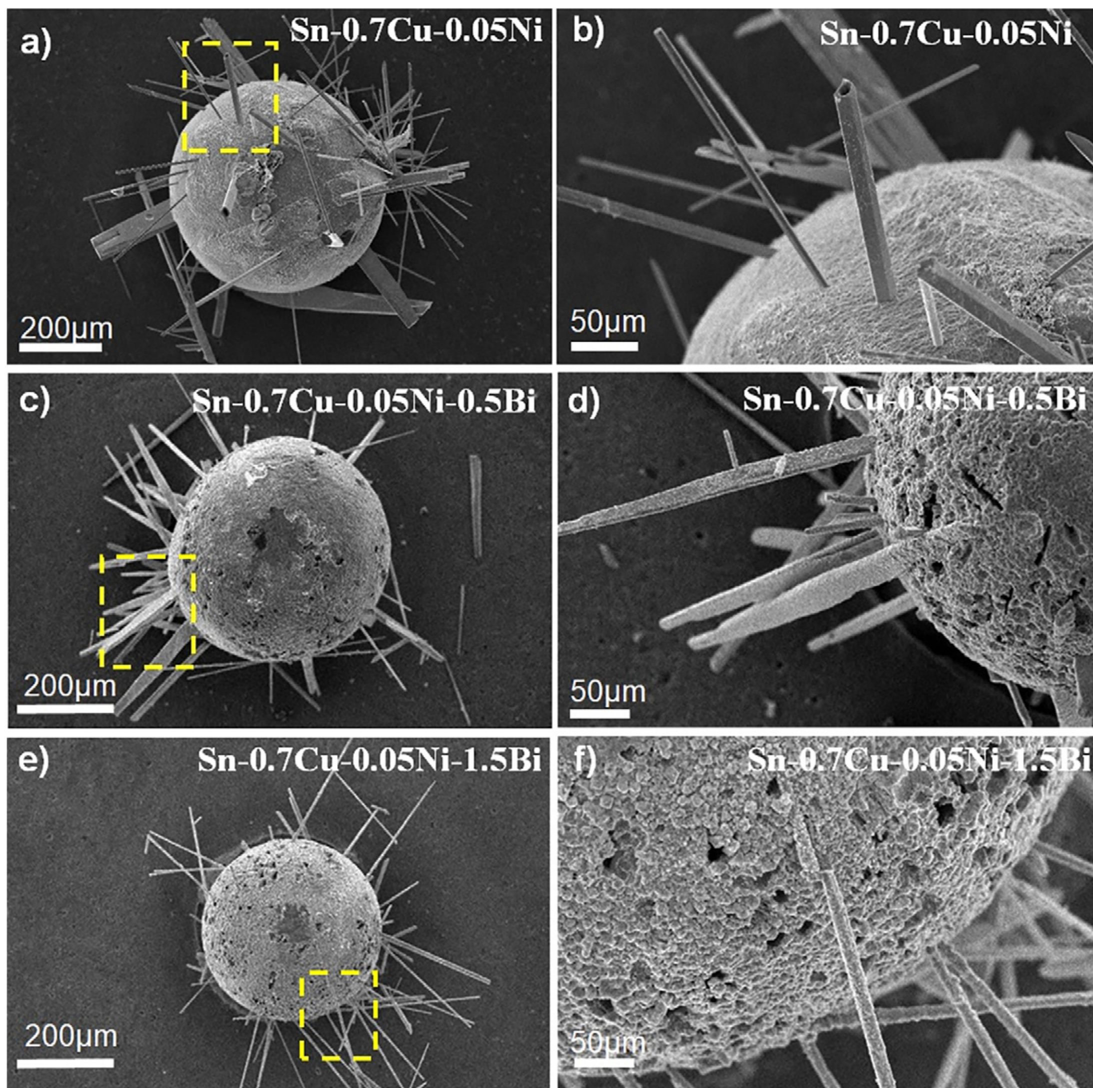

Fig. 12. Top view of the primary $(Cu,Ni_6)Sn_5$ crystal that was formed in the bulk solder (β-Sn had been shallow etched). The Sn-0.7Cu-0.05Ni at low (a) and high (b) magnification. Sn-0.7Cu-0.05Ni-0.5Bi at low (c) and high (d) magnification. Sn-0.7Cu-0.05Ni-1.5Bi at low (e) and high (f) magnification.

profile and growth behaviour of the primary $(Cu,Ni)_6Sn_5$ that were plotted in Fig. 6, the primary $(Cu,Ni)_6Sn_5$ was found to have grown with time during the Sn-0.7Cu-0.05Ni and Sn-0.7Cu-0.05Ni-1.5Bi solidification processes. By setting the experimental time as 0 s at a melting point of 227 °C, the primary $(Cu,Ni)_6Sn_5$ phase for the Sn-0.7Cu-0.05Ni (Fig. 6a) was discovered to have begun growing at 130 s prior to stoping nucleation at 187 s, while those of the Sn-0.7Cu-0.05Ni-1.5Bi (Fig. 6b) were found to have nucleated and grew at 111 s before ceasing at ~135 s. This implies that the $(Cu,Ni)_6Sn_5$ intermetallic compound in the Sn-0.7Cu-0.05Ni-1.5Bi experienced an earlier growth than that of the $(Cu,Ni)_6Sn_5$ in the Sn-0.7Cu-0.05Ni solder alloy. The addition of the Bi element could have reduced the undercooling and consequently promoted the occurrence of nucleation behaviours in the solidification process of the liquid solder alloys [26].

The shorter time taken for the nucleation of $(Cu,Ni)_6Sn_5$ intermetallic compound in the Sn-0.7Cu-0.05Ni-1.5Bi solder alloy at 24 s as compared to the 57 s that was exhibited by the $(Cu,Ni)_6Sn_5$ intermetallic compound in the Sn-0.7Cu-0.05Ni solder alloy had also suggested the rapid solidification affecting the nucleation growth time and inhibiting the tip growth [0001] of the $(Cu,Ni)_6Sn_5$ intermetallic compound in the Sn-0.7Cu-0.05Ni and Sn-0.7Cu-0.05Ni-1.5Bi solder alloys, respectively.

In Fig. 7(a–f), the primary (Cu,Ni)6Sn5 in the Sn-0.7Cu-0.05Ni/Cu was found to have experienced a nucleation phase from the experimental time of 130 s–187 s at ~191 °C–217 °C during the cooling process, while the real-time observation of the Sn-0.7Cu-0.05Ni-1.5Bi/Cu solder alloy reaction at the experimental times of 88 s–201 s depicted in Fig. 8(a–f) show the primary (Cu,Ni)6Sn5 intermetallic as nucleating with an experimental time of 111 s–135 s at between 227 °C and 240 °C.

The primary IMC (Cu,Ni)6Sn5 that had nucleated and grew with increased solidification time would eventually appear as sediments due to the difference in the liquid density levels. As per Figs. 7 and 8, the primary (Cu,Ni)6Sn5 was not only found to have experienced a more rapid formation in the Sn-0.7Cu-0.05Ni-1.5Bi than the Sn-0.7Cu-0.05Ni. The addition of a 1.5 wt% Bi element was also found to have resulted in smaller-sized primary (Cu,Ni)6Sn5 intermetallics. Since it was assumed that the Bi element had dissolved in the supersaturation of the primary β-Sn phase due to its high solubility level [22], the Bi element that was present within the β-Sn matrix might have then reduced the length of the (Cu,Ni)6Sn5 IMC particles. It also shows that Bi not just reduces the length of primary (Cu,Ni)6Sn5 but also increases the numbers of primary (Cu,Ni)6Sn5 which reflects the nucleation of primary $(Cu,Ni)_6Sn_5$. It was found that 64% increase in the number of crystals nucleated after the addition of 1.5 wt% Bi. This show that the primary (Cu,Ni)6Sn5 is more numerous in Sn-0.7Cu-0.05Ni-1.5Bi solder alloy. This observation coincided with the one reported by Salleh et al. [35], where it was posited that the addition of the Ni element in the Sn-0.7Cu as reducing

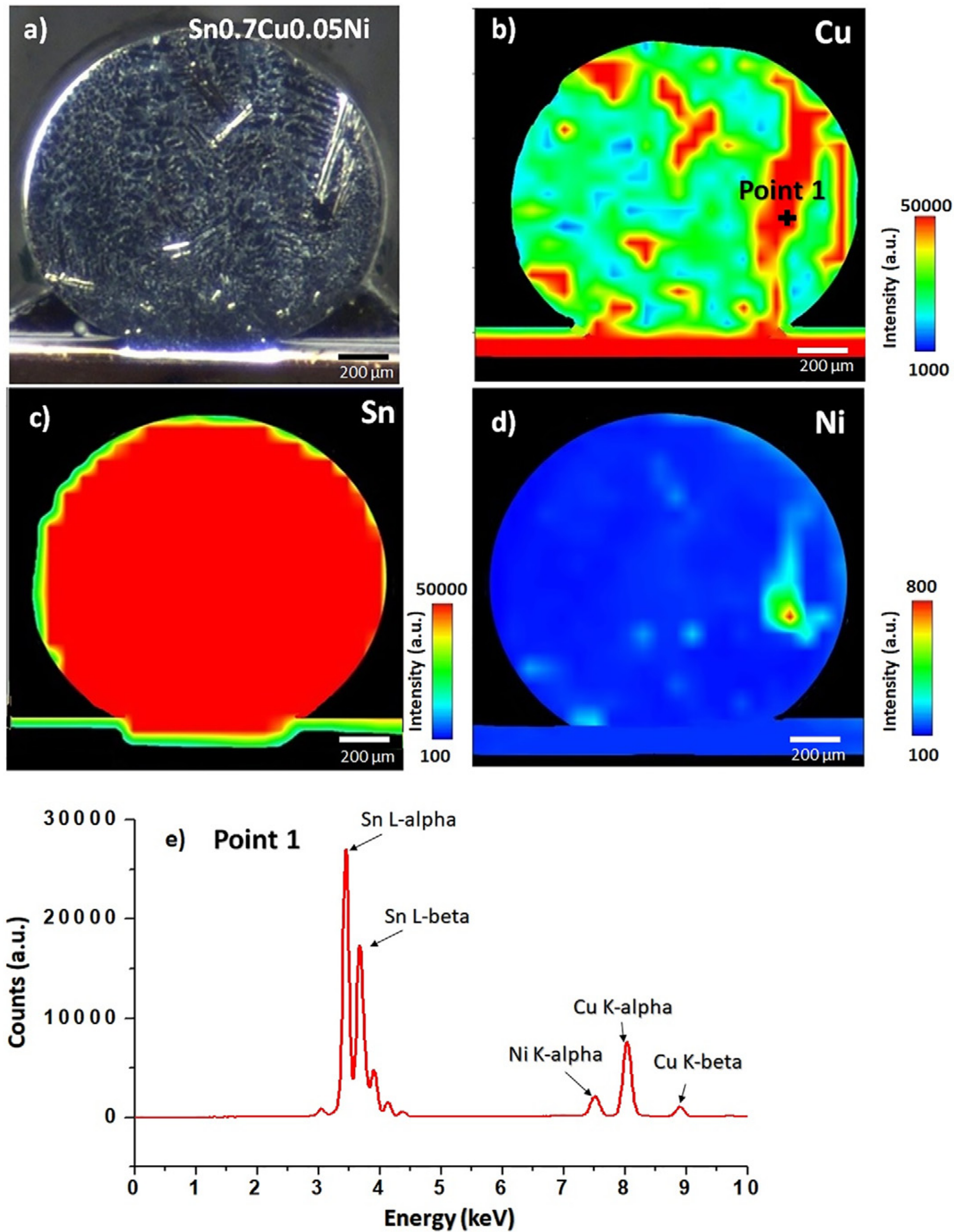

Fig. 13. (a) The micro-XRF mapping area image of Sn-0.7Cu-0.05Ni, (b) mapping distribution of the Cu element, (c) mapping distribution of the Sn element, (d) mapping distribution of the Ni element and (e) spectrum point analysis at point 1.

the growth and the particle size of the primary IMCs. Similarly, the addition of a 0.05 wt% Ni element in the Sn-0.7Cu also refined the Cu_6Sn_5 scallops to (Cu,Ni)6Sn5 while also decreasing its average diameter, making them much smaller than those of the Cu_6Sn_5.

Since the primary (Cu,Ni)6Sn5 crystals had grown as single faceted rods [0001], the tip growth length of the primary $(Cu,Ni)_6Sn_5$ crystal as a function of time was measured, while the length of the primary Sn-0.7Cu-0.05Ni and Sn-0.7Cu-0.05Ni-1.5Bi intermetallics on the Cu substrates were determined by using the Image-J software. The investigation on the growth of the primary (Cu,Ni)6Sn5 on solder alloy was conducted on five individual (Cu,Ni)6Sn5 intermetallic particles shown in Fig. 9 (a and b). The solidification kinetics of the primary (Cu,Ni)6Sn5 crystals in the Sn-0.7Cu-0.05Ni/Cu and Sn-0.7Cu-0.05Ni-1.5Bi/Cu joints quantified in Fig. 9 (c and d) indicated the length of the primary (Cu,Ni)6Sn5 intermetallic particles in the Sn-0.7Cu-0.05Ni+1.5Bi of 322–524–µm as being smaller than that of the Sn-0.7Cu-0.05Ni (445–963–µm). While conducting a study on the Sn-0.7Cu, Salleh et al. [35] point out that the size of the primary Cu6Sn5 to be 1300–1800 μm^2, while the Cu6Sn5 in Sn-3.0Ag-0.5Cu [30] measured 900 μm^2. The size differences of the primary Cu6Sn5 intermetallic particles that formed between the Sn-0.7Cu [35] and Sn-3.0Ag-0.5Cu [30] as well as those of Sn-0.7Cu-0.05Ni and Sn-0.7Cu-0.05Ni+1.5Bi solder joints, implies that the smaller particle sizes contributed to the solder joints' enhanced mechanical properties. This observation of the smaller primary IMC size in the matrix as decreasing the solder's brittleness and consequently, its mechanical strength was also reported by other studies [35].

The (Cu,Ni)6Sn5 particles in the Sn-0.7Cu-0.05Ni/Cu joint were found to have grown at a rate of 29.18–µm/s to a length of 500–µm before

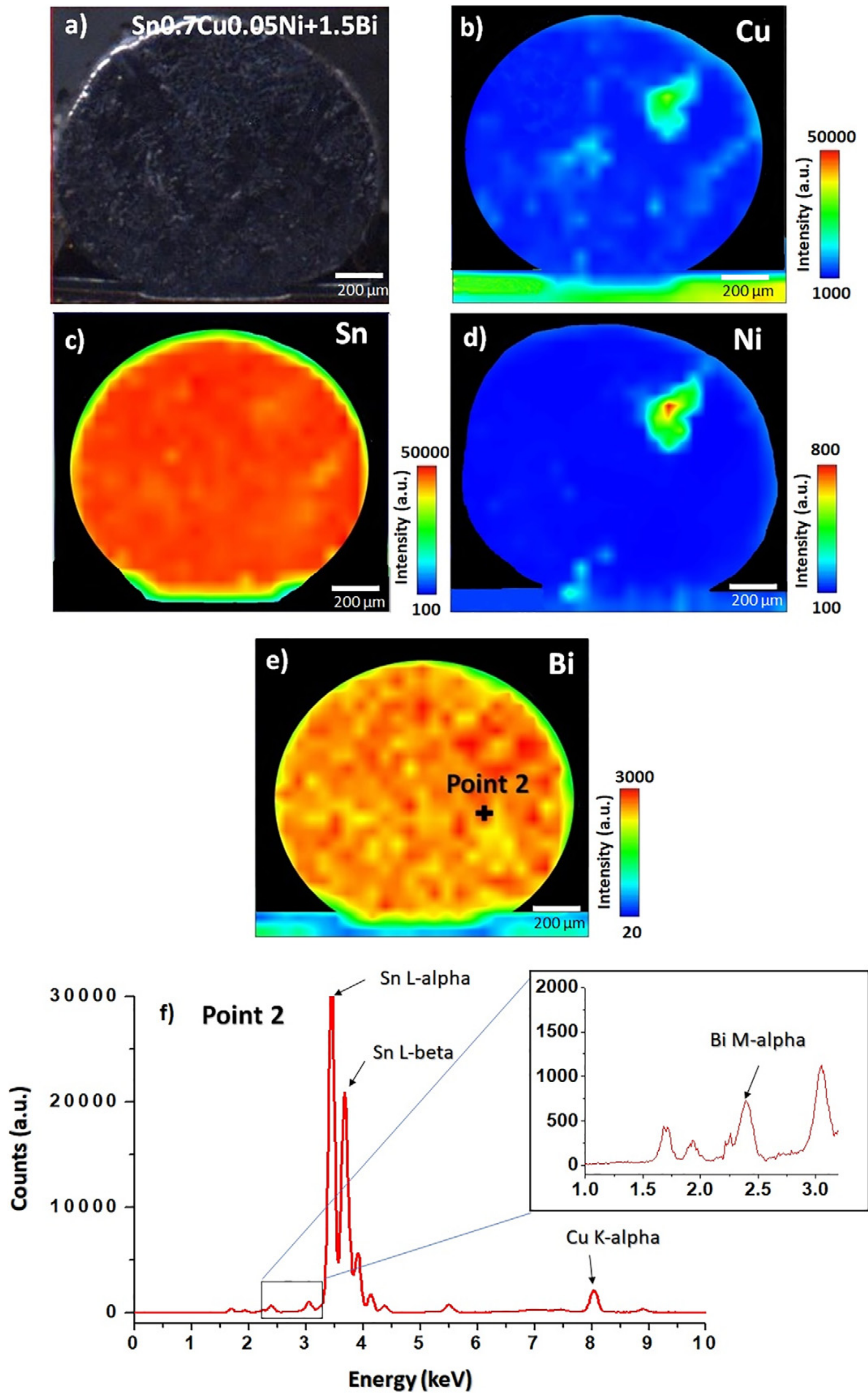

Fig. 14. (a) The micro-XRF mapping area image of Sn-0.7Cu-0.05Ni-1.5Bi, (b) mapping distribution of the Cu element, (c) mapping distribution of the Sn element, 0(d) mapping distribution of the Ni element, (e) mapping distribution of the Bi element and (e) spectrum point analysis at point 2.

slowing down at 9.26–μm/s to 800–μm. The (Cu,Ni)6Sn5 rods in the Sn-0.7Cu-0.05Ni+1.5Bi/Cu joint were discovered to have been smaller and grew at a rate of 44.0–μm/s for 300–μm before decelerating at 5.71–μm/s to a final length of 500–μm. In the case of the Sn-3.0Ag-0.5Cu/Cu joint solder [30], the primary Cu_6Sn_5 was observed to have experienced a speed of 9.8 μm/s and a length of 600 μm before halting growth. These

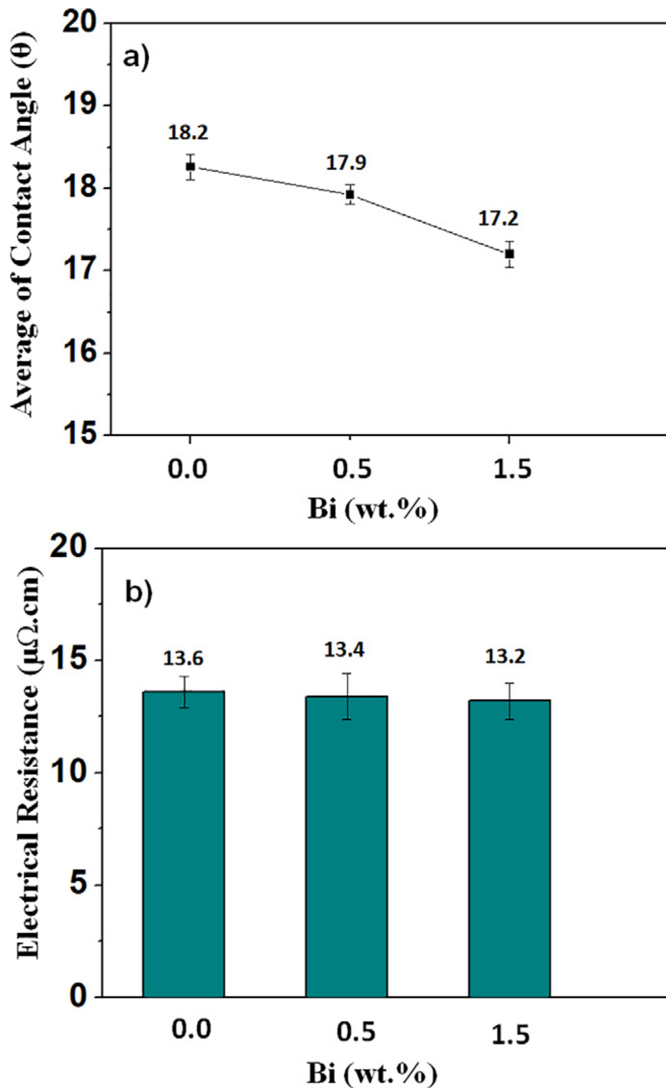

Fig. 15. (a) Wetting angle of the Sn-0.7Cu-0.05Ni-xBi solder alloy on the Cu substrate and (b) electrical Resistance of the Sn-0.7Cu-0.05Ni-xBi solder alloys.

observations implies that the rapid tip growth rate of the (Cu,Ni)6Sn5 primary intermetallic in the Sn-0.7Cu-0.05Ni-1.5Bi/Cu resulted from the addition and present Bi element promoted a faster solute field formation ahead of the (Cu,Ni)6Sn5 tip, thereby increasing the (Cu,Ni)6Sn5 growth rate of the Bi-contained solder. In addition, the primary (Cu,Ni)6Sn5 in Sn-0.7Cu-0.05Ni-1.5Bi grew earlier with a faster growth rate in shorter time compared to Sn-0.7Cu-0.05Ni (without Bi). As it can be seen in Fig. 9, the primary (Cu,Ni)6Sn5 in Sn-0.7Cu-0.05Ni grew at a slower rate but however had sufficient time to grow to a larger size. On the other hand, primary (Cu,Ni)6Sn5 in Sn-0.7Cu-0.05Ni-1.5Bi grew at a faster rate and solidifies earlier and hence resulted in a smaller size compared to primary (Cu,Ni)6Sn5 in Sn-0.7Cu-0.05Ni. Since the tips of the (Cu,Ni) 6Sn5 grew as faceted rods, their vector could then be quantified by a single vector of the growth vector direction [0001] by using a single origin. It can be seen in Fig. 10 that the (Cu,Ni)6Sn5 tips of both the Sn-0.7Cu-0.05Ni and Sn-0.7Cu-0.05Ni-1.5Bi as experiencing a random orientation, lacking a designated growth direction(s).

The post mortem of the Sn-0.7Cu-0.05Ni/Cu and Sn-0.7Cu-0.05Ni-1.5Bi/Cu solder joint samples that had undergone the *in-situ* experiments shown in Fig. 11 were then cross-sectioned to reveal the primary IMC image of the β-Sn and $(Cu,Ni)_6Sn_5$ phases that is present in the solder bulk region (Fig. 11b) as well as the interfacial $(Cu,Ni)_6Sn_5$ IMC between the solder and the Cu substrate in the Sn-0.7Cu-0.05Ni/Cu solder joint (Fig. 11c). The cross-sectioned SEM images of the respective Sn-0.7Cu-0.05Ni-1.5Bi/Cu whole solder joint, as well as the primary and interfacial $(Cu,Ni)_6Sn_5$ IMCs, are also depicted in Fig. 11d-f.

The SEM-EDX that was utilised to identify the IMC phase compositions of the formed primary and interfacial IMCs at the Cu substrate confirmed that the addition of the Bi element to have not significant influenced the chemical composition of the IMCs phases [44]. However, its appearance in the bulk solder was found to have provided a solid solution strengthening mechanism on the solder joint system. As per this post mortem observation, it can be surmised that the addition of the Bi element had no apparent effect on the β-Sn refinement and the interfacial IMC layer thickness level.

The primary $(Cu,Ni)_6Sn_5$ particles were then deep-etched to study the size morphologies present in the Sn-0.7Cu-0.05Ni and Sn-0.7Cu-0.05Ni-xBi solder joints. The reduction in the initial mixture of the large and small primary $(Cu,Ni)_6Sn_5$ particles, as depicted in the case of Sn-0.7Cu-0.05Ni (Fig. 12a and b) due to the addition of the 1.5 wt% Bi element is shown in Fig. 12 (e and f) correspond to the previous supposition of the Bi element, decreasing the size of the primary $(Cu,Ni)_6Sn_5$ IMC.

3.4. Phase distributions

The composition and distribution of the elements in the Sn-0.7Cu-0.05Ni solder balls samples were then analysed and compared using the synchrotron micro-XRF mapping. Fig. 13 shows the results of micro-XRF in Sn-0.7Cu-0.05Ni solder balls, where the elemental map of the Sn, Cu and Ni are presented. Higher intensity indicates a higher concentration of a particular element. Spot analysis was also conducted on the selected areas, as per point 1 (Fig. 13b) showing the existence of the primary (Cu,Ni)6Sn5. As per Fig. 13b and d, the Cu and Ni elements are dispersed throughout the Sn-grain and are likely identified as (Cu, Ni)6Sn5 intermetallics.

The distribution of the smaller sized and area of the (Cu,Ni)6Sn5 intermetallics in the Sn-0.7Cu-0.05Ni with the added Bi element depicted in Fig. 14 not only imply that the Sn-0.7Cu-0.05Ni-Bi has a lower Cu concentration level than that of the Sn-0.7Cu-0.05Ni solder alloy, but the Bi element was also found to be evenly distributed in the β-Sn region (point 2), as shown in Fig. 14e and f.

3.5. Wettability properties

The wettability of a solder, dictated by the contact angle (θ) to the Cu substrate, is essential. A small contact angle (<90°) would denote a high wettability, and vice versa. As per Fig. 15 (a), the contact angle of the Sn-0.7Cu-0.05Ni was found to have decreased by 5.8% from 18.2° to 17.2° due to the addition of a 1.5 wt% Bi element, implying that the Bi element not only improves the wettability of the liquid but also has the potential for decreasing the surface tension of the liquid solder alloy.

The decrease in the contact angle can be attributed to the surface tension of the liquid solder alloy, where the spread of the liquid or wettability is influenced by the higher molecule force of attraction from a lower liquid surface tension or by increasing the solid's surface energy. This similar finding was outlined by Liu et al. [45], where they reported that the addition of a small amount of Bi element in the Sn-0.3Ag-0.7Cu solder as significantly improving the liquid's wettability due to its reduction of the subsequent surface tension.

3.6. Electrical conductivity

Since the solder also serves as an electrical support for forming the required electrical connections within a circuit, it must, therefore, possess excellent electrical conductivity. As per Fig. 15 (b), the addition of the Bi element was found to have no significant effect on the electrical resistance, although the bulk resistance decreased from 13.4 μΩ cm to 13.2 μΩ cm when the added Bi element increased from 0.5 wt% to 1.5 wt%. The Bi was reported to have a room temperature solubility limit in Sn at

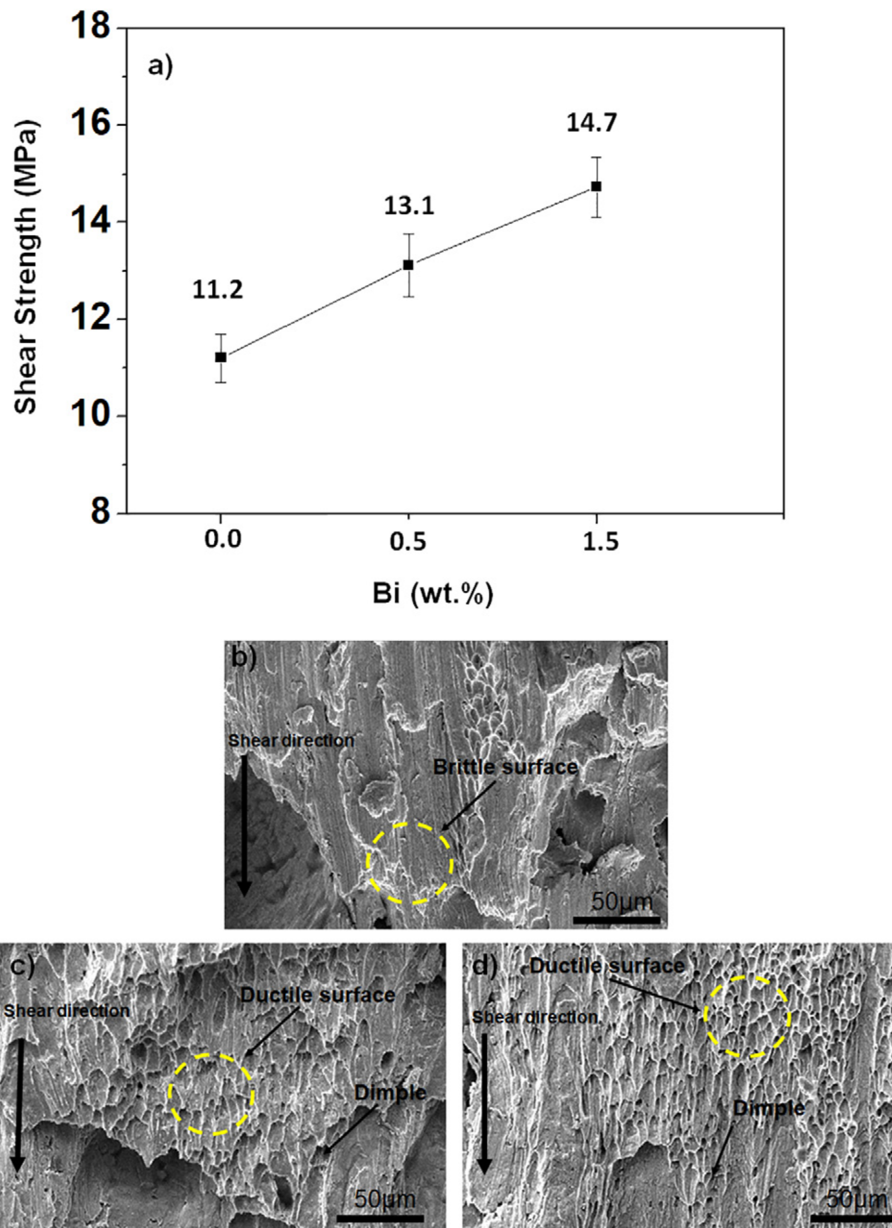

Fig. 16. (a) Shear force that indicates the shear strength of the Sn-0.7Cu-0.05Ni-xBi solder joint. The shear test fractography of specimens b) Sn-0.7Cu-0.05Ni, c) Sn-0.7Cu-0.05Ni-0.5Bi, d) Sn-0.7Cu-0.05Ni-1.5Bi.

approximately 1.8 wt% [46]. At above the solubility limit, Bi precipitation will form and could increase the electrical resistivity of the Sn alloy. Most findings reported that with additions of Bi above the solubility limit would increase the electrical resistivity of Sn alloys [47,48].

The substitutional solid solution, formed from the Bi element and the Sn in the primary β-Sn dendrites of the solder alloy was also discovered to have reduced the alloy's resistance level due to the increased β-Sn size, as well as the decreased Sn activity in the chemical reaction that took place between Sn and Cu. This decrease can therefore, be attributed to decreased size of $(Cu,Ni)_6Sn_5$ particles that had a higher electrical resistance level (17.5 μΩ cm) than that of the β-Sn (12.0 μΩ cm) [49]. While investigating the influence of the added Zn in the Sn-10Sb-Cu solder alloy, Lashin et al. [50] reported the increase in its electrical resistance level as being attributed to the formation of the intermetallic compounds (SbSn and Cu_3Sn). Since the electrical resistance results had revealed a small electrical resistance difference due to the present of the Bi element, this had therefore confirmed the Sn-0.7Cu-0.05Ni-xBi as an electrical connection (role) of a solder joint.

3.7. Shear strength and fracture energy of the solder joints

The mechanical performance of the Sn-0.7Cu-0.05Ni-xBi/Cu solder joint was measured by determining its shear strength. The addition of a 0.5 wt% Bi element to the Sn-0.7Cu-0.05Ni solder joint was found to have increased its average shear strength by 14.5% and those of the Sn-0.7Cu-0.05Ni-1.5Bi by 23.9% to 14.7 MPa, as shown in Fig. 16 (a). Higher Bi concentration above its solubility limit at 1.8 wt% will increase Bi precipitation in Sn and thus, the shear strength will keep increasing as reported by Shen et al. [51] and Tateyama et al. [52]. However, due to the brittleness of Bi precipitates, it has been demonstrated by Liu et al. [27] on Sn-Ag-Cu based solder that the addition of Bi above 3 wt% in the solder alloy is harmful to elongation.

It is a fact that the interfacial IMC, flux void formation, Kirkendall void formation, and the primary intermetallic of the solder joint matrix dictates the strength of a solder joint [2,53]. The shear strength in this study, however, increased due to the solid solution strengthening effect of the Bi element dissolved in the β-Sn matrix. The increased shear

strength could also be attributed to the increased crystal lattice parameters from the added Bi element, as suggested by Liu et al. [54], as well as the solid solution strengthening mechanism reported in the improved shear strength of the Sn-Ag-Cu [55]. It can, therefore, be surmised that the dissolution of the Bi element in the matrix improved the shear performance of the solder joint. This also suggests that Sn-0.7Cu-0.05-1.5Bi solder alloy is the best composition in the context of high strength solder for the automotive and defence industries and other harsh environments. This new solder alloy can also utilise the existing parameters for the soldering process.

The fractography comparison of the Sn-0.7Cu-0.05Ni at multiple added Bi percentages was conducted using the SEM, as shown in Fig. 16(b–d), where the fine dimples that had appeared on the Sn-0.7Cu-0.05Ni-0.5Bi and Sn-0.7Cu-0.05Ni-1.5Bi specimens had confirmed not only the occurrence of plastic deformation during the fracture process but also the fact that the number of dimples as being correlated to the Bi content percentages. The fracture on the Sn-0.7Cu-0.05Ni was also found to have a more dimple-like fracture on the 1.5Bi added solders.

The observations mentioned above can be partially attributed to the solid solution strengthening mechanism of the Bi element in the bulk solder, which curbed the formation of the IMC phases, particularly those of the $(Cu,Ni)_6Sn_5$. For this reason, and since the long primary Cu_6Sn_5 IMC protrusions are known to be undesirable and has the potential for damaging reliabilities [30] as per the *in-situ* tensile tests of the Sn-3Ag-0.5Cu/Cu conducted by Tian et al. [36], the smaller IMC particles with more obstacles per unit area to the slipping of dislocations are instead seen as producing a stronger strengthening effect in the solder joint, which implies that the shear strength of the Sn-0.7Cu-0.05Ni-xBi can be improved by decreasing the size of the $(Cu,Ni)_6Sn_5$ particles, as well as the strengthening the β-Sn.

4. Conclusion

The effect of the added Bi element on the microstructure, electrical resistance, wettability and shear strength of the Sn-0.7Cu-0.05Ni solder alloy was elucidated in this paper. It can be concluded that:

a) The added Bi element did not significantly influence the layers' thickness and the interfacial IMC layer size of the Sn-0.7Cu-0.05Ni solder.
b) The micro-XRF analysis confirmed the excellent dispersion of the Bi element in the β-Sn, which decreases the $(Cu,Ni)_6Sn_5$ eutectic area fraction and increases the β-Sn dendrite area fraction of the Sn-0.7Cu-0.05Ni solder joint.
c) The (Cu,Ni)6Sn5 primary intermetallic in the Sn-0.7Cu-0.05Ni-1.5Bi/Cu solder joint was discovered to have undergone a more rapid early growth rate (44.0 μm/s) than that of the Sn-0.7Cu-0.05Ni/Cu solder joint (29.18 μm/s).
d) The addition of 1.5%Bi element was found to have resulted in a 3% reduction of the Sn-0.7Cu-0.05Ni electrical resistance and a 5.8% contact reduction, at a superior wettability performance.
e) The average shear strength of the Sn-0.7Cu-0.05Ni (11.2 MPa) and the Sn-0.7Cu-0.05Ni-0.5Bi solder joints increased by a respective of 14.5% (13.1 MPa) and 23.9% (14.7 MPa) due to the addition of 1.5 wt% of the Bi element.

CRediT authorship contribution statement

M.I.I. Ramli: Writing - original draft. **M.A.A. Mohd Salleh:** Writing - original draft, Writing - review & editing. **H. Yasuda:** Investigation. **J. Chaiprapa**: Investigation. **K. Nogita:** Writing - original draft, Writing - review & editing.

Acknowledgements

The authors gratefully acknowledge the financial support from the Universiti Malaysia Perlis (UniMAP)-Nihon Superior Ltd collaboration research project (Grant No: 2016/10/0001) and the fundamental research grant scheme (FRGS) (FRGS/1/2017/TK05/UNIMAP/02/7) (9003-00635) from the Ministry of Higher Education, Malaysia. The *in-situ* synchrotron radiation experiment was performed at the Japan Synchrotron Radiation Research Institute (JASRI) at the BL20B2 and BL20XU beamline of the SPring-8 Synchrotron, under proposal No: 2016B1319 and 2017B1519. The in-situ observations were supported by a Grant-in-Aid for Scientific Research (S) (No. 17H06155), JSPS, Japan. The μ-XRF trace element mapping technique was performed at the Synchrotron Light Research Institute (SLRI), Thailand, under project ID: 3774 and 3774-7. The authors also acknowledge Dr Kentaro Uesugi, Dr. Akihisa Takeuchi at SPring-8, Prof Hideyuki Yasuda and his research group from the Department of Materials Science and Engineering, Kyoto University, for their experimental assistance, Mr Keith Sweatman at Nihon Superior Co. Ltd, and Dr Stuart McDonald for his valuable discussion.

References

[1] T. Ventura, Y.H. Cho, C. Kong, A.K. Dahle, formation of intermetallics in Sn-0.9Cu and Sn-0.7Cu-0.08Ni solders, J. Electron. Mater. 40 (2011) 1403–1408.
[2] M.A.A.M. Salleh, S.D. McDonald, K. Nogita, Effects of Ni and TiO2 additions in as-reflowed and annealed Sn0. 7Cu solders on Cu substrates, J. Mater. Process. Technol. 242 (2017) 235–245.
[3] Y. Wang, G. Wang, K. Song, K. Zhang, Effect of Ni addition on the wettability and microstructure of Sn2.5Ag0.7Cu0.1RE solder alloy, Mater. Des. 119 (2017) 219–224.
[4] T. Maeshima, H. Ikehata, K. Terui, Y. Sakamoto, Effect of Ni to the Cu substrate on the interfacial reaction with Sn-Cu solder, Mater. Des. 103 (2016) 106–113.
[5] K. Kanlayasiri, T. Ariga, Physical properties of Sn58Bi-xNi lead-free solder and its interfacial reaction with copper substrate, Mater. Des. 86 (2015) 371–378.
[6] A.A. El-Daly, A.M. El-Taher, Improved strength of Ni and Zn-doped Sn-2.0Ag-0.5Cu lead-free solder alloys under controlled processing parameters, Mater. Des. 47 (2013) 607–614.
[7] E.A. Eid, A.N. Fouda, E.-S.M. Duraia, Effect of adding 0.5 wt% ZnO nanoparticles, temperature and strain rate on tensile properties of Sn-5.0 wt% Sb-0.5 wt% Cu(SSC505) lead free solder alloy, Mater. Sci. Eng. A 657 (2016) 104–114.
[8] W. Ng, G. Zeng, T. Nishimura, K. Sweatman, S.D. McDonald, K. Nogita, The Beneficial Effect of Zn Additions on the Microstructure of SnCu and SnCuNi Solder Joints to Cu Substrates, ICEP-IAAC, 2015.
[9] M.H. Mahdavifard, M.F.M. Sabri, D.A. Shnawah, S.M. Said, I.A. Badruddin, S. Rozali, The effect of iron and bismuth addition on the microstructural, mechanical, and thermal properties of Sn-1Ag-0.5 Cu solder alloy, Microelectron. Reliab. 55 (2015) 1886–1890.
[10] S.A. Belyakov, J.W. Xian, K. Sweatman, T. Nishimura, T. Akaiwa, C.M. Gourlay, Influence of bismuth on the solidification of Sn-0.7 Cu-0.05 Ni-xBi/Cu joints, J. Alloy. Comp. 701 (2017) 321–334.
[11] B.K.D. Barman, S.P. Singh, P. Kumar, Processing and mechanical behavior of Cu-Bi alloys with high volume fraction of Bi: suitability for high temperature soldering application, Mater. Sci. Eng. A 666 (2016) 339–349.
[12] M.I.I. Ramli, M.S.S. Yusof, M.A.A.M. Salleh, R.M. Said, K. Nogita, Influence of Bi addition on wettability and mechanical properties of Sn-0.7 Cu solder alloy, Solid State Phenom. 273 (2018) 27–33.
[13] X. Yan, K. Xu, J. Wang, X. Wei, W. Wang, Effect of P and Ge Doping on Microstructure of Sn-0.3Ag-0.7Cu/Ni-P Solder Joints, Soldering & Surface Mount Technology, 2016 28.
[14] H.R. Kotadia, O. Mokhtari, M. Bottrill, M.P. Clode, M.A. Green, S.H. Mannan, Effect of Al and Zn alloying elements on Sn-3.8 Ag-0.7 Cu and Sn-3.6 Ag solder reaction with Cu and Ni (P) substrate, Advanced Packaging Materials: Microtech, 2010 APM'10 International Symposium on: IEEE 2010, pp. 17–21.
[15] L. Yang, Y. Zhang, J. Dai, Y. Jing, J. Ge, N. Zhang, Microstructure, interfacial IMC and mechanical properties of Sn-0.7Cu-xAl (x = 0-0.075) lead-free solder alloy, Mater. Des. 67 (2015) 209–216.
[16] L.F. Li, Y.K. Cheng, G.L. Xu, E.Z. Wang, Z.H. Zhang, H. Wang, Effects of indium addition on properties and wettability of Sn-0.7Cu-0.2Ni lead-free solders, Mater. Des. 64 (2014) 15–20.
[17] C.M. Gourlay, K. Nogita, J. Read, A.K. Dahle, Intermetallic formation and fluidity in Sn-rich Sn-Cu-Ni alloys, J. Electron. Mater. 39 (2010) 56–69.
[18] T. Ventura, C.M. Gourlay, K. Nogita, T. Nishimura, M. Rappaz, A.K. Dahle, The influence of 0-0.1 wt.% Ni on the microstructure and fluidity length of Sn0.7Cu-xNi, J. Electron. Mater. 37 (2008) 32–39.
[19] K. Nogita, Stabilisation of Cu_6Sn_5 by Ni in Sn-0.7Cu-0.05Ni lead-free solder alloys, Intermetallics 18 (2010) 145–149.
[20] K.M. Kareh, C. O'Sullivan, T. Nagira, H. Yasuda, C.M. Gourlay, Dilatancy in semi-solid steels at high solid fraction, Acta Mater. 125 (2017) 187–195.
[21] S.A. Belyakov, C.M. Gourlay, Effect of Bi and in on microstructure formation in Sn-3Ag-3Bi-3In/Cu and/Ni solder joints, Key Eng. Mater.: Trans. Tech. Publ. (2016) 142–151.

[22] M.H. Mahdavifard, M.F.M. Sabri, S.M. Said, D.A. Shnawah, I.A. Badruddin, S. Rozali, Effects of Fe and Bi minor alloying on mechanical, thermal, and microstructural properties of Sn-0.7 Cu solder alloy, J. Electron. Mater. (2016) 1–10.
[23] T.Y. Kang, Y.Y. Xiu, L. Hui, J.J. Wang, W.P. Tong, C.Z. Liu, Effect of bismuth on intermetallic compound growth in lead free solder/Cu microelectronic interconnect, J. Mater. Sci. Technol. 27 (2011) 741–745.
[24] S.A. Belyakov, J. Xian, K. Sweatman, T. Nishimura, T. Akaiwa, C.M. Gourlay, Influence of bismuth on the solidification of Sn-0.7Cu-0.05Ni-xBi/Cu joints, J. Alloy. Comp. (2016).
[25] K. Nogita, M.A.A.M. Salleh, S. Smith, Y. Wu, S.D. McDonald, A.G.A. Razak, et al., Effects of bismuth in Sn-Cu based solder alloys and interconnects, Trans. Jpn Inst. Electron. Pack. 10 (2017)E17-E1003-1-E17–7.
[26] X. Hu, Y. Li, Y. Liu, Z. Min, Developments of high strength Bi-containing Sn0.7Cu lead-free solder alloys prepared by directional solidification, J. Alloy. Comp. 625 (2015) 241–250.
[27] Y. Liu, F. Sun, X. Li, Effect of Ni, Bi concentration on the microstructure and shear behavior of low-Ag SAC-Bi-Ni/Cu solder joints, J. Mater. Sci. Mater. Electron. 25 (2014) 2627–2633.
[28] Z. Xuan, F. Mao, Z. Cao, T. Wang, L. Zou, In situ observation on the solidification of Sn-10Cu hyperperitectic alloy under direct current field by synchrotron microradiography, J. Alloy. Comp. (2017).
[29] C.M. Gourlay, K. Nogita, A.K. Dahle, Y. Yamamoto, K. Uesugi, T. Nagira, et al., In situ investigation of unidirectional solidification in Sn-0.7 Cu and Sn-0.7 Cu-0.06 Ni, Acta Mater. 59 (2011) 4043–4054.
[30] M.A.A.M. Salleh, C.M. Gourlay, J.W. Xian, S.A. Belyakov, H. Yasuda, S.D. McDonald, et al., In situ imaging of microstructure formation in electronic interconnections, Sci. Rep. 7 (2017) 40010.
[31] J.W. Xian, S.A. Belyakov, M. Ollivier, K. Nogita, H. Yasuda, C.M. Gourlay, Cu_6Sn_5 crystal growth mechanisms during solidification of electronic interconnections, Acta Mater. 126 (2017) 540–551.
[32] H.T. Ma, L. Qu, M.L. Huang, L.Y. Gu, N. Zhao, L. Wang, In-situ study on growth behavior of Ag3Sn in Sn-3.5 Ag/Cu soldering reaction by synchrotron radiation real-time imaging technology, J. Alloy. Comp. 537 (2012) 286–290.
[33] M.L. Huang, F. Yang, N. Zhao, Z. Zhang, J. In situ study on dissolution and growth mechanism of interfacial Cu6Sn5 in wetting reaction, Mater. Lett. 139 (2015) 42–45.
[34] Y. Takamatsu, H. Esaka, K. Shinozuka, Formation mechanism of eutectic Cu6Sn5 and Ag3Sn after growth of primary β-Sn in Sn-Ag-Cu alloy, Mater. Trans. 52 (2011) 189–195.
[35] M.A.A.M. Salleh, S.D. Mcdonald, C.M. Gourlay, S.A. Belyakov, H. Yasuda, K. Nogita, Effect of Ni on the formation and growth of primary Cu_6Sn_5 intermetallics in Sn-0.7 wt.%Cu solder pastes on Cu substrates during the soldering process, J. Electron. Mater. 45 (2016) 154–163.
[36] Y. Tian, W. Liu, R. An, W. Zhang, L. Niu, C. Wang, Effect of intermetallic compounds on fracture behaviors of Sn3. 0Ag0. 5Cu lead-free solder joints during in situ tensile test, J. Mater. Sci. Mater. Electron. 23 (2012) 136–147.
[37] M.A.A.M. Salleh, S.D. McDonald, C.M. Gourlay, H. Yasuda, K. Nogita, Suppression of Cu_6Sn_5 in TiO_2 reinforced solder joints after multiple reflow cycles, Mater. Des. 108 (2016) 418–428.
[38] V. Solé, E. Papillon, M. Cotte, P. Walter, J. Susini, A multiplatform code for the analysis of energy-dispersive X-ray fluorescence spectra, Spectrochim. Acta B At. Spectrosc. 62 (2007) 63–68.
[39] N. Zhao, Y. Zhong, M.L. Huang, H.T. Ma, W. Dong, Growth kinetics of Cu_6Sn_5 intermetallic compound at liquidsolid interfaces in Cu/Sn/Cu interconnects under temperature gradient, Sci. Rep. 5 (2015) 1–12.
[40] Y.C. Chan, A.C.K. So, J.K.L. Lai, Growth kinetic studies of Cu-Sn intermetallic compound and its effect on shear strength of LCCC SMT solder joints, Mater. Sci. Eng. B55 (1998) 5–13.
[41] K. Nogita, T. Nishimura, Nickel-stabilized hexagonal $(Cu, Ni)_6Sn_5$ in Sn-Cu-Ni lead-free solder alloys, Scr. Mater. 59 (2008) 191–194.
[42] E. Hodulova, M. Palcut, E. Lechovic, B. Simekova, K. Ulrich, Kinetics of intermetallic phase formation at the interface of Sn-Ag-Cu-X (X= Bi, In) solders with Cu substrate, J. Alloy. Comp. 509 (2011) 7052–7059.
[43] S. Belyakov, T. Nishimura, T. Akaiwa, K. Sweatman, C. Gourlay, Role of Bi in microstructure formation of Sn-Cu-Ni based BGAs on Cu metallizations, Electronics Packaging (ICEP), 2017 International Conference on: IEEE 2017, pp. 232–236.
[44] B. Ali, M.F.M. Sabri, I. Jauhari, N.L. Sukiman, Impact Toughness, Hardness and Shear Strength of Fe and Bi Added Sn-1Ag-0.5Cu Lead-free Solders, Microelectronics Reliability, 2016.
[45] Y. Liu, F.L. Sun, T.L. Yan, W.G. Hu, Effects of Bi and Ni addition on wettability and melting point of Sn-0.3Ag-0.7 Cu Low-Ag Pb-free solder, Electronic Packaging Technology & High Density Packaging, 2008 ICEPT-HDP 2008 International Conference on: IEEE 2008, pp. 1–4.
[46] D.B. Witkin, Influence of microstructure on quasi-static and dynamic mechanical properties of bismuth-containing lead-free solder alloys, Mater. Sci. Eng. A 532 (2012) 212–220.
[47] H.A. Jaffery, M.F.M. Sabri, S. Rozali, M.H. Mahdavifard, D.A. Shnawah, Effect of temperature and alloying elements (Fe and Bi) on the electrical resistivity of Sn-0.7 Cu solder alloy, RSC Adv. 6 (2016) 58010–58019.
[48] A.B. El-Bediwi, A. El-Shafei, M. Kamal, Influence of Adding Bi\or Bi-in on Structure and Required Properties of Tin-Copper Lead Free Solder Alloy, 2014.
[49] N.A.A.M. Amin, D.A. Shnawah, S.M. Said, M.F.M. Sabri, H. Arof, Effect of Ag content and the minor alloying element Fe on the electrical resistivity of Sn–Ag–Cu solder alloy, J. Alloy. Comp. 599 (2014) 114–120.
[50] A.R. Lashin, M. Mossa, A. El-Bediwi, M. Kamal, Study of some physical properties of the rapidly solidified Sn-Sb-Cu-Zn alloys, Mater. Des. 43 (2013) 322–326.
[51] J. Shen, Y. Pu, D. Wu, Q. Tang, M. Zhao, Effects of minor Bi, Ni on the wetting properties, microstructures, and shear properties of Sn-0.7 Cu lead-free solder joints, J. Mater. Sci. Mater. Electron. 26 (2015) 1572–1580.
[52] K. Tateyama, H. Ubukata, Y. Yamaoka, K. Takahashi, H. Yamada, M. Saito, Effects of Bi content on mechanical properties and bump interconnection reliability on Sn-Ag solder alloys, Int. J. Microcircuits Electron. Packag. 23 (2000) 131–137.
[53] H.T. Lee, M.H. Chen, Influence of intermetallic compounds on the adhesive strength of solder joints, Mater. Sci. Eng. A 333 (2002) 24–34.
[54] C.-Y. Liu, M.-H. Hon, M.-C. Wang, Y.-R. Chen, K.-M. Chang, W.-L. Li, Effects of aging time on the mechanical properties of Sn-9Zn-1.5 Ag-xBi lead-free solder alloys, J. Alloy. Comp. 582 (2014) 229–235.
[55] L. Yang, S. Fenglian, Y. Miaosen, Shear strength and brittle failure of low-Ag SAC-Bi-Ni solder joints during ball shear test, Electronic Packaging Technology (ICEPT), 2013 14th International Conference on: IEEE 2013, pp. 750–753.